One-Pot Synthesis of Block Copolymers in Supercritical Carbon Dioxide: A Simple Versatile Route to Nanostructured Microparticles

James Jennings,[†] Mariana Beija,[†] Alexandre P. Richez,[†] Samuel D. Cooper,[†] Paul E. Mignot,[†] Kristofer J. Thurecht,[†,‡] Kevin S. Jack,[§] and Steven M. Howdle*[,†]
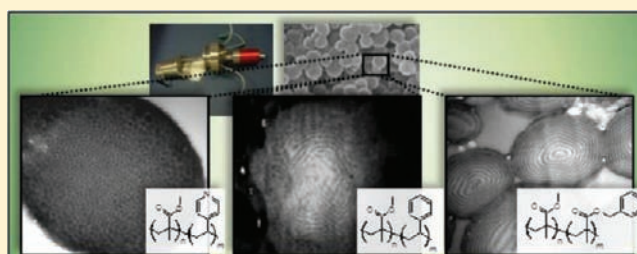
[†]School of Chemistry, University of Nottingham, University Park, Nottingham, NG7 2RD, U.K.

[‡]Australian Institute for Bioengineering and Nanotechnology and Centre for Advanced Imaging, The University of Queensland and [§]Centre for Microscopy and Microanalysis, Brisbane, Australia

S *Supporting Information*

ABSTRACT: We present a one-pot synthesis for well-defined nanostructured polymeric microparticles formed from block copolymers that could easily be adapted to commercial scale. We have utilized reversible addition—fragmentation chain transfer (RAFT) polymerization to prepare block copolymers in a dispersion polymerization in supercritical carbon dioxide, an efficient process which uses no additional solvents and hence is environmentally acceptable. We demonstrate that a wide range of monomer types, including methacrylates, acrylamides, and styrenics, can be utilized leading to block copolymer materials that are amphiphilic (e.g., poly(methyl methacrylate)-*b*-poly(*N*,*N*-dimethylacrylamide)) and/or mechanically diverse (e.g., poly(methyl methacrylate)-*b*-poly(*N*,*N*-dimethylaminoethylmethacrylate)). Interrogation of the internal structure of the microparticles reveals an array of nanoscale morphologies, including multilayered, curved cylindrical, and spherical domains. Surprisingly, control can also be exerted by changing the chemical nature of the constituent blocks and it is clear that selective CO_2 sorption must strongly influence the block copolymer phase behavior, resulting in kinetically trapped morphologies that are different from those conventionally observed for block copolymer thin films formed in absence of CO_2.

INTRODUCTION

Composite polymer particles featuring internal ordered structures are vital for applications such as impact modifiers, fillers, and stiffening agents.[1] Recently, such nanostructured particles have shown significant promise for more advanced applications such as catalyst supports,[2] photonic crystals,[3,4] high density optical and magnetic data storage and encryption, and as spherical dielectric resonators.[5] We present here a facile and environmentally acceptable route to these interesting and desirable materials.

Block copolymers are particularly important to a wide range of applications because they provide a controllable route to highly ordered structures on the nanoscale by exploiting their ability to self-assemble in the bulk, solution phase and in thin films.[6−9] These assemblies arise from energetic incompatibility of the two blocks, and the covalent bond between them which prevent macroscopic phase separation. The structures observed in the melt or in thin films can be influenced by the relative sizes of the two blocks (also known as mass or volume fraction), among other variables, to attain spherical, cylindrical, gyroid and lamellar type morphologies.[6−8]

Within nano- or microparticles, three-dimensional spherical confinement of diblock copolymers has been observed[10−13] leading to analogous morphologies in the form of onion-like layers, curved cylinders, and spheres.[11] There are currently four published routes to such structured block copolymer particles:

(1) solvent-absorbing/solvent-releasing method (SARM);[14−16] (2) self-organized precipitation (SORP);[17] (3) evaporation-induced self-assembly via emulsion[11,12] or aerosol;[18] and (4) (mini)emulsion.[19−21] SARM requires the internal reorganization of preformed monodisperse particles (around 1 μm in size) obtained from seeded emulsion polymerization and produces morphologies from core−shell to onion-like or spherical domains by first swelling the particles with an organic solvent (such as toluene) and then releasing it by slow evaporation.[14−16] In the SORP method, nano- or microparticles are prepared by evaporation of a good solvent from a solution of preformed block copolymer (or a mixture of block copolymer and homopolymer) from a mixture of good and poor solvents.[13,17,22,23] This method yields particles of several nanometers to a few micrometers containing different kinetically trapped morphologies.[13,22] The thermodynamically preferred morphology can be obtained by further temperature[24] or solvent[25] annealing. The evaporation-induced self-assembly method is similar to SORP, but requires a polymer dispersed in an organic solvent in water, stabilized with a surfactant, prior to solvent evaporation.[11,12] All of these methods have significant drawbacks; they are time-consuming (evaporation steps can last up to one week), require multiple steps, use volatile organic

Table 1. Macromolecular Characteristics of the Block Copolymers Synthesized by RAFT Dispersion Polymerization in scCO$_2$[a]

polymer structure	PMMA mass fraction[b]	$M_{n,theo}$[c] (kg mol^{-1})	$M_{n,exp}$[d] (kg mol^{-1})	Đ[d]	D_n[e] /μm	internal morphology[f]	T_g[g] /°C (PMMA)	T_g[g] /°C (2nd block)
PMMA (45)-b-P4VP (15)	0.67	60	69	1.99	2.24 ± 0.55	Sph	128	150
PMMA (30)-b-P4VP (30)	0.49	60	68	1.98	1.87 ± 0.43	Sph	130	154
PMMA (15)-b-P4VP (45)	0.25	60	61	1.71	0.71 ± 0.27	L	121	150
PMMA (30)-b-PSt (30)	0.55	60	57	1.68	1.02 ± 0.36	Cyl	124	103
PMMA (75)-b-PBzMA (25)	0.78	100	83	1.32	3.28 ± 0.84	None	105	
PMMA (50)-b-PBzMA (50)	0.51	100	89	1.31	1.74 ± 0.54	L	112	57
PMMA (45)-b-PDMAEMA (15)	0.83	60	48	1.24	1.89 ± 0.59	Sph	96	51
PMMA (30)-b-PDMAEMA (30)	0.58	60	44	1.33	n/s[h]	L	109	29
PMMA (75)-b-PDMA (25)	0.71	100	94	1.58	3.00 ± 0.77	Sph	115	79
PMMA (50)-b-PDMA (50)	0.47	100	94	1.69	1.76 ± 0.40	L/Sph	115	70

[a]Reactions performed with [MMA + Monomer$_2$] = 2.5 M, RAFT/AIBN = 1:1 or 1:0.5, 5 wt % PDMS-MA (with respect to both monomers) in 60 mL autoclave at 65 °C and 4000 psi (275 bar). [b]Calculated from NMR integral of each polymer (P1, P2) by: P1 × MW$_{Monomer1}$/[(P2 × MW$_{Monomer2}$) + (P1 × MW$_{Monomer1}$)]. [c]$M_{n,theo}$ was calculated by: [Monomer$_1$]/[RAFT] × MW$_{Monomer1}$ × Conversion + [Monomer$_2$]/[RAFT] × MW$_{Monomer2}$ × Conversion. [d]Dispersity determined by GPC in chloroform/ethanol/triethylamine (90/10/0.5 by volume)[45] or THF at 40 °C, against PMMA standards. [e]Particle size determined by SEM, with at least 120 particles measured, [f]Sph = spherical, L = lamellar, Cyl = cylindrical. [g]Measured by either DSC or DMA. [h]Nonspherical particles, no measurements possible.
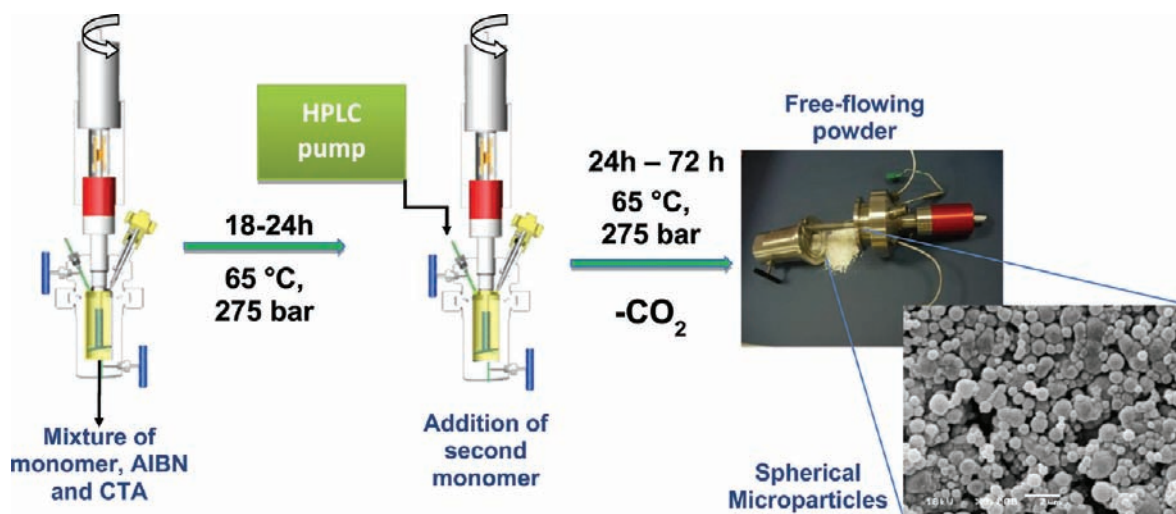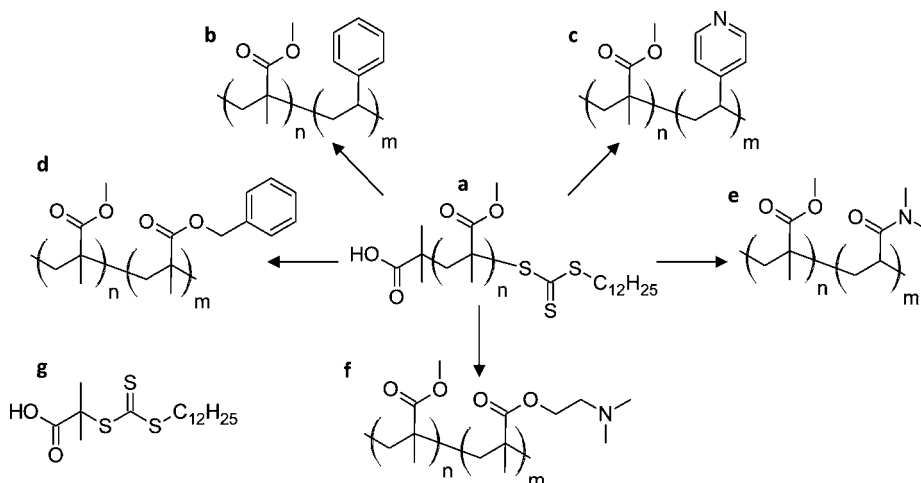

Figure 1. One-pot method for the clean preparation of nanostructured polymeric microparticles in scCO$_2$.

solvents, and mostly use preprepared block copolymers synthesized by anionic polymerization. For all of these reasons, the processes could not easily be scaled for industrial production. The fourth alternative, (mini)emulsion synthesis appears to be a more sustainable method for the preparation of nanostructured polymer particles. There has been significant recent progress using controlled radical polymerizations (CRP) such as RAFT,[26] NMP,[19,27] ATRP,[20] and AGET-ATRP[21] in aqueous (mini)emulsion to prepare block copolymers that lead to nanostructured nano- and microparticles. However, the choice of polymers is limited to hydrophobic, and inefficient formation of block copolymers (blocking efficiency) can be observed.[21] The complexities associated with the addition of CRP in an emulsion polymerization mechanism may also require additional steps, such as emulsion seeding.[21] There are also very recent examples of controlled dispersion polymerizations in water, but these are limited because there are only a few water-soluble monomers that can lead to water insoluble polymers.[28]

The development of a simple, adaptable, and environmentally friendly method for the production of such nanostructured microparticles is a high priority, and here we report the use of supercritical carbon dioxide (scCO$_2$) to facilitate syntheses that cannot easily be achieved in conventional solvents. This is timely given the global focus on CO$_2$ through carbon capture and sequestration, and the potential to exploit this plentiful resource to replace our use of conventional solvents. There is already a significant body of work in polymer synthesis and polymer processing using scCO$_2$[29,30] and the high solubility of most monomers, and the poor solubility of most polymers in scCO$_2$ makes it an ideal solvent for dispersion polymerization.[31] Moreover, there are significant advantages over conventional solvents because CO$_2$ is essentially inert to free radical reactions (specifically chain transfer to solvent); eliminates solvent residues; produces dry, free-flowing powders consisting of spherical microparticles; and the heterogeneous polymerization process is aided by the low viscosity and high diffusivity of scCO$_2$.[32,33] The solvent has even been extended to monomers which are water-reactive and for the formation of

Scheme 1. Chemical Structures of the Block Copolymers Synthesized by RAFT Dispersion Polymerization in scCO$_2$ from (a) PMMA-RAFT Precursor, (b) PMMA-b-PSt, (c) PMMA-b-P4VP, (d) PMMA-b-PBzMA, (e) PMMA-b-PDMA, (f) PMMA-b-PDMAEMA, and the RAFT Agent Used in all Syntheses, (g) DATC

incompatible polymer composites.[34] Recent developments of controlled radical polymerizations in scCO$_2$,[35−38] including RAFT, show that scCO$_2$ can be applied to the synthesis of block copolymers.[37] In this paper, we describe a facile, one-pot, solvent-free method for the preparation of nanostructured block copolymer microparticles by sequential RAFT-controlled dispersion polymerization. Moreover, we expand the range of monomers that are available to form block copolymer microparticles, which to date have been limited to hydrophobic polyacrylates, polymethacrylates, or polystyrenics. The block copolymers synthesized here are structurally diverse, and we demonstrate changes in morphology that can be introduced simply by manipulating copolymer composition and chemical structure. We believe that our approach has several genuine advantages over existing routes to block copolymers and provides nanostructure microparticles which are very difficult or tedious to produce by existing methods.

■ EXPERIMENTAL SECTION

Materials. S-Dodecyl-S'-(α,α'-dimethyl-α''-acetic acid)-trithiocarbonate (DATC) was synthesized following literature procedure.[39] α-Azobisisobutyronitrile (AIBN, Wako, 97%) was purified by recrystallizing twice in methanol. Methyl methacrylate (MMA, Fisher, >99%), benzyl methacrylate (BzMA, Alfa Aesar, 98%), N,N-dimethylacrylamide (DMA, Alfa Aesar, >99%), 2-dimethylaminoethyl methacrylate (DMAEMA, Alfa Aesar, 97%), and styrene (St, Alfa Aesar, 99%) were purified by eluting through a basic alumina and 4-vinylpyridine (4VP, Alfa Aesar, 96%) was distilled prior to use. Poly(dimethylsiloxane monomethyl methacrylate) (PDMS-MA, ABCR, M_n = 10 000 g·mol^{-1}), CDCl$_3$ (Aldrich), iodine (Fisher) and ruthenium tetroxide (Acros, 0.5% solution in water) were used as received. HPLC grade THF (Fisher), chloroform (Aldrich), and ethanol (Fluka) were used without further purification. Agar 100 resin (Agar Scientific) was used as received, and a formulation of medium hardness was used for embedding samples.

One-Pot Block Copolymer Synthesis. A typical procedure (Table 1, entry 1) involved use of an in-house built high pressure autoclave (60 mL) (Figure 1), which was charged with RAFT agent (DATC, Scheme 1, 0.245 mmol), AIBN (0.122 mmol), and a macromonomer stabilizer (PDMS-MA, 5 wt % wrt both monomers). PDMS-MA is well-known to act as a grafting steric stabilizer in scCO$_2$.[40] The autoclave was degassed by purging with CO$_2$ at 2 bar for 30 min, while MMA (112.2 mmol) was degassed by bubbling with argon, before being added to the autoclave. The vessel was then sealed

and pressurized to 50 bar, heated to 65 °C, and the pressure topped up to 275 bar (27.5 MPa). The reaction mixture was stirred for 18−24 h, after which time a sample was taken for analysis by GPC and SEM, from the bottom of the autoclave by needle valve.[41] 4VP (36.35 mmol) was then degassed for 30 min, and transferred to a vial containing AIBN (0.061 mmol) to be degassed for a further 10 min. In the cases where full monomer conversion was not achieved, CO$_2$ was flushed through the reactor for ∼10 min, before the pressure was reduced to <200 bar. The monomer was then added to the top of the vessel by HPLC pump (Gilson). After a further 24−72 h, the temperature was lowered to ambient, and the pressure reduced by venting the autoclave over a period of ∼30 min. All products were collected as dry, pale yellow, free-flowing powders (Figure 1).

Preparation of Thin Films. Thin films for small-angle X-ray scattering (SAXS) analysis were solvent cast from tetrahydrofuran (THF). Typically, 500 μL of polymer solution (∼100 mg/mL) was deposited onto a Kapton window and then annealed at 40 °C for 2 days to remove THF. SAXS was measured on the resulting film as cast and then again following subsequent annealing above the glass transition temperatures (T_g) of one of the blocks.

Analysis. Block copolymers were analyzed by ^{1}H NMR in CDCl$_3$ in order to determine the mass fraction of blocks (see Supporting Information (SI) Figures 6−10). Measurements were recorded on a Bruker DPX 300 MHz spectrometer. Gel Permeation Chromatophy (GPC) analysis was carried out on a Polymer Laboratories PL GPC 50 in a mixture of chloroform/ethanol/triethylamine (90/10/0.5 by volume) for PMMA-b-P4VP, PMMA-b-PDMA, and PMMA-b-PDMAEMA copolymers, or a PL GPC 120 in THF for other copolymers, at a flow rate of 1 mL/min and 40 °C. Columns were calibrated with PMMA narrow standards. For SEM, samples were mounted on an aluminum stub and sputter-coated with gold, before being imaged on a Jeol JSM 6060LV. Particle size was determined by measurements taken in ImageJ software.

Samples for TEM were prepared by embedding in epoxy resin (Agar 100) and setting at 60 or 30 °C depending on the T_g of the constituent polymers. Thin sections (100 nm) were cut by ultramicrotoming with a diamond knife (Leica Diatome Ultra 45°) and were placed on copper grids. PMMA-b-P4VP and PMMA-b-PDMA copolymers were stained with I$_2$ vapor for ∼2 h prior to imaging, in order to enhance the contrast in the images by adsorbing to P4VP and PDMA domains. In addition, PMMA-b-PBzMA and PMMA-b-PSt copolymers were stained with RuO$_4$ vapor for ∼1 h prior to imaging, a stain which adsorbs selectively to PBzMA and PSt domains. All samples were also imaged without staining to demonstrate that the same features are present (see SI Figure 2). T_g values were obtained by Differential Scanning Calorimetry (DSC) on a
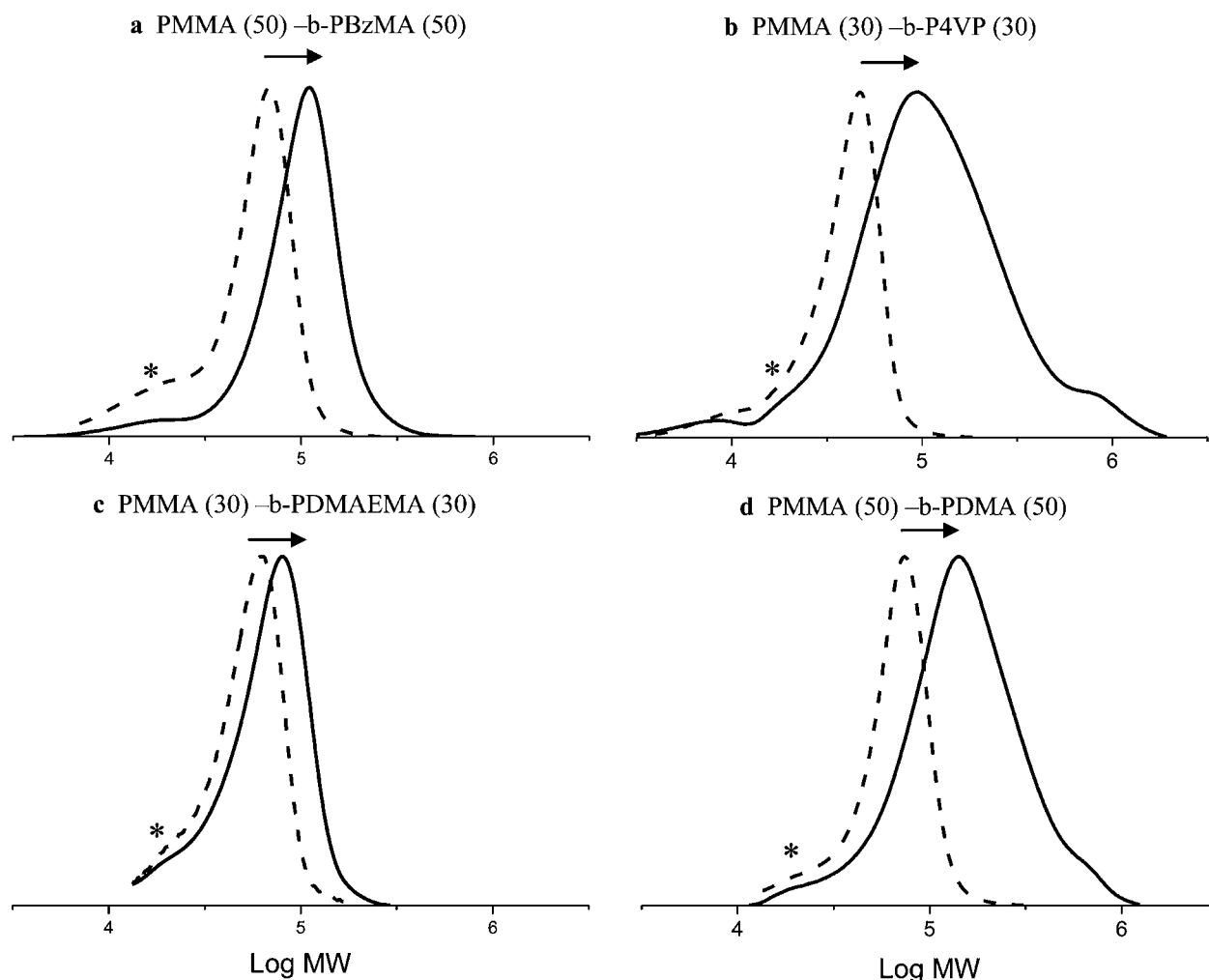
Figure 2. GPC chromatograms (RI traces, response has been normalized) to the first block (PMMA macro-RAFT, dashed line) and, in the corresponding block copolymers in (solid line): (a) PMMA (50)-*b*-PBzMA (50), (b) PMMA (30)-*b*-P4VP (30), (c) PMMA (30)-*b*-PDMAEMA (30), (d) PMMA (50)-*b*-PDMA (50). The low molecular weight shoulders (*) are attributed to residual PDMS-MA stabilizer ($M_n \approx 10$ kg/mol).

TA Q2000 in aluminum pans, at a heating rate of 10 °C/min or by Dynamic Mechanical Analysis (DMA) on a Triton Technology TT DMA, in powder pockets, at a heating rate of 1 °C/min.

SAXS data were measured on the SAXS/WAXS beamline at the Australian Synchrotron. The data were collected at a camera length of 7.2 m, using a *Pilatus* 1M camera, and at a photon energy of 10 keV, to give a total q range of ca. 0.003–0.8 Å^{-1}. Powdered samples of the polymers were contained in 1.5 mm quartz capillaries and all measurements were collected at 25 °C. Annealing experiments were carried out in situ by heating the powdered samples to various temperatures between Kapton foils in a Linkam heating stage. Particular temperature ranges for each sample are described in the Supporting Information. The 2D scattering profiles were reduced to 1D curves using standard procedures and background corrected by subtracting the scattering from an empty quartz capillary or Kapton foils, as appropriate, after correction for the relative transmissions of the samples and the background.

■ RESULTS AND DISCUSSION

1. Synthesis and Characterization of Block Copolymers. A trithiocarbonate RAFT agent, DATC (Scheme 1g) was used to control the dispersion polymerization of the first PMMA block. This RAFT agent has been reported to exert good control over radical polymerizations of a range of vinylic monomer classes.[39] On completion of the first block, a small sample of the PMMA microparticulate product was taken and

the second monomer was generally added at 80–90% conversion of the first MMA block. The key reason for this is because the degree of livingness in any CRP is well-known to deteriorate with time due to the increase in chain–chain termination, especially by disproportionation in the case of MMA, and other undesirable side reactions.[42] However, the conversion should not be too low, otherwise there will be formation of a central "statistical block" consisting of a mixture of MMA and the second monomer, which has been shown to affect block copolymer phase behavior.[19] In our scCO$_2$ process, we have also developed a method to remove residual MMA by flushing the reactor through with a flow of CO$_2$ for ~10 min in such a way that we maintain the dispersion, but also allow for injection of the second monomer and growth of the second block without contamination by MMA. For monomers exhibiting lower k_p values, for example, the methacrylates and styrene, additional initiator was also injected simultaneously to ensure complete growth of the second block. Finally, the second block was grown to high conversion (>90% in most cases) in order to minimize residual monomer, before the reaction was quenched by cooling and release of CO$_2$ pressure.

We targeted a range of chemically distinct block copolymers (Scheme 1), while varying the mass fraction of PMMA in each. Our block copolymer syntheses (Table 1) demonstrated
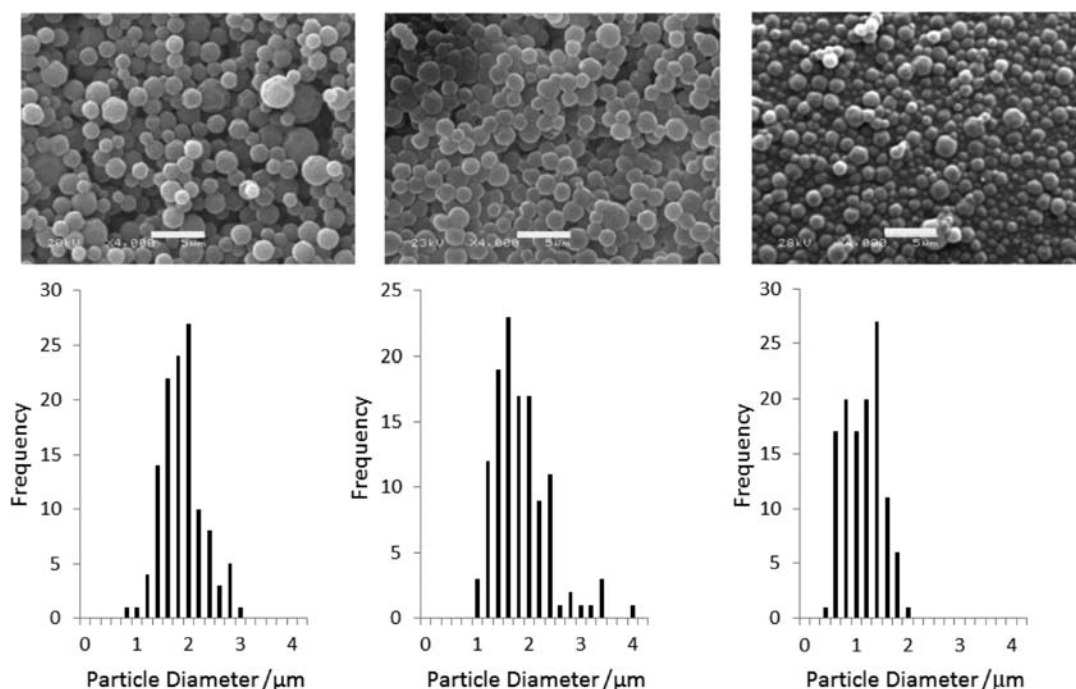
Figure 3. SEM (above) with particle size histogram (below) of PMMA-*b*-PDMA block copolymer particles (a) PMMA (50)-*b*-PBzMA (50), (b) PMMA (50)-*b*-PDMA (50), and (c) PMMA (30)-*b*-PSt (30). Scale bar in each image is 5 μm. Particle size histograms were obtained from measurements of at least 120 particles.

excellent molecular weight control with values close to those targeted, and relatively low dispersities for methacrylate copolymers (mostly Đ < 1.5), indicating successful RAFT-controlled dispersion polymerization. However, low dispersity cannot be achieved with acrylamides and styrenics, because of their higher tendency to terminate by combination, particularly under monomer starved conditions.[21] This is evident in the GPC traces of these copolymers, in which high molecular weight shoulders are visible (Figure 2). The polymers PMMA-*b*-PBzMA and PMMA-*b*-PDMAEMA showed molecular weights lower than targeted. This is most likely due to a considerable difference between their hydrodynamic volume and those of the PMMA standards used for GPC analysis. Shoulders at low molecular weight (∼10 kg/mol) were observable in most cases, and were attributed to unreacted PDMS-MA stabilizer that remained in the sample. However, this could be removed by postpolymerization processing (see SI Figure 5).

These polymerizations require a higher initiator concentration than in conventional homogeneous RAFT polymerizations. We previously reported this for polymerization of MMA by RAFT in scCO$_2$, and attributed this to increased initiator-initiator terminations occurring because of the low viscosity and high diffusivity of scCO$_2$, and radical partitioning between the particle and continuous phase.[43,44] However, the observed molecular weights still agree well with those targeted based on [Monomer]$_0$/[RAFT]$_0$, the higher initiator concentration does not appear to increase the number of propagating chains and depress the final M_n, and the system retains chain-end fidelity.

In all cases, block copolymer formation is evidenced by a shift toward higher molecular weight of the GPC traces from the PMMA macro-RAFT agent to the final product (Figure 2). However, we recognize that chain end functionality is never maintained at 100%, and we would expect some contamination of the final block copolymer product with a small amount of "dead" homopolymer PMMA chains that were unable to undergo chain extension with the second monomer. The quantification of this is discussed in more detail later.

This level of control is not always observed in other heterogeneous CRP processes. For example, one-pot syntheses of block copolymer particles by seeded AGET-ATRP in water can show poor efficiency in reinitiation of polymer chains, probably as a result of the complexity of the emulsion mechanism resulting in poor transfer of monomer into the polymer particle.[21] Additionally, final products often show a higher dispersity (Đ > 2) due to lack of control over side reactions such as termination and branching.[21,46]

The low viscosity and high diffusivity of scCO$_2$ ensures efficient plasticization of PMMA by scCO$_2$[32,37] and hence allows excellent access of the growing chain ends and the RAFT agent to incoming monomer. This ensures that the locus of the polymerization remains in the microparticle and leads to efficient block copolymer formation. In addition, the reversible chain transfer mechanism[47] ensures the RAFT agent is attached to a polymer chain throughout the reaction and therefore remains within the particle. This is an advantage over other CRP mechanisms, where the deactivating moiety is free to leave the particle and enter the continuous phase when not attached to a polymer chain. In other work, additional reagents were required to overcome this issue; for example, a ligating monomer was required for dispersion ATRP in scCO$_2$ to capture the copper complex and prevent its transfer to the continuous phase.[48]

2.1. Particle Morphology and Phase Behavior.
External Morphology. The dispersion polymerizations produced spherical particles for both the PMMA first block (see SI Figure 3) and final block copolymer product (Figure 3). This retention of sphericity upon formation of a second block demonstrates that steric stabilization is maintained successfully
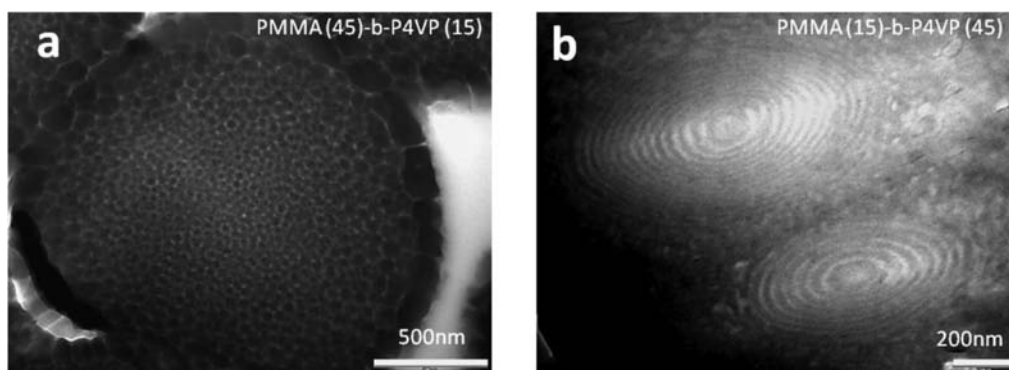
Figure 4. TEM images of block copolymers (a) PMMA (45)-*b*-P4VP (15) (spherical) and PMMA (15)-*b*-P4VP (45) (lamellar). The dark domains are from the iodine-stained P4VP.
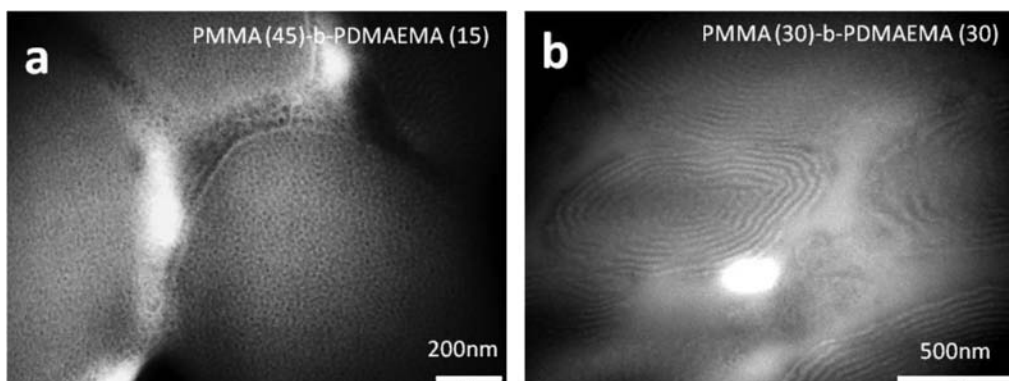

Figure 5. TEM images of block copolymers (a) PMMA (45)-*b*-PDMAEMA (15) and PMMA (30)-*b*-PDMAEMA (30). The dark domains are from the iodine-stained PDMAEMA.

in the presence of the second monomer, which on addition may act as a cosolvent or as a nonsolvent for the PMMA particles and/or stabilizer. The only exception was for PMMA (30)-*b*-PDMAEMA (30), in which the final microparticles were nonspherical, but still particulate. This is likely a consequence of the low T_g of PDMAEMA, which leads to some foaming of the polymer upon depressurization and has been observed previously[40] for synthesis of PMMA-s-PDMAEMA copolymers in scCO$_2$ where both monomers were present from the beginning of the reaction, resulting in the formation of particles with a low average T_g. In the case of the block copolymer, low T_g domains are trapped within a matrix of the higher T_g polymer (PMMA). This facilitates the formation of discrete particles of PMMA-*b*-PDMAEMA, instead of the monoliths that were observed for PMMA-s-PDMAEMA at the same monomer ratio. Good distributions of particle sizes were typically observed (Figure 3), along with an increase in particle size from the PMMA sample to the final copolymer product (see SI Figure 4) in all but one case. This demonstrates that there is little or no additional particle nucleation on addition of the second monomer, and that the block copolymer is growing within the PMMA particles.

2.2. Internal Morphology. Interrogation of the internal morphology of the block copolymer microparticles by TEM (Figures 4−6) reveals a diverse range of nanostructures that arise from phase segregation of the incompatible blocks. Extensive studies on thin films have determined that morphological variation is expected for block copolymer systems as the relative mass fraction of the two segments is altered: from lamellar, to cylindrical and spherical domains.[6]

Some 3-dimensional analogues have also been observed when under spherical confinement in nano and microparticles.[11]

In our one-pot system, we demonstrate the ability to manipulate the internal particle nanostructure simply by altering the ratio of the two blocks. For example, the PMMA-*b*-P4VP system can be shifted from spherical domains of P4VP in PMMA to multilayered lamellar ("onion-like") morphology by changing the mass fraction of PMMA from 0.67 to 0.25, respectively (Figure 4).

The morphology of the block copolymer PMMA-*b*-PDMAEMA could also be manipulated upon changing the relative mass fraction of the two blocks (Figure 5). Spherical domains of PDMAEMA were observed in a PMMA matrix when PMMA mass fraction was 0.83, whereas a lamellar morphology was evident upon changing the mass fraction of PMMA to 0.58. This is close to what we would expect from a classical block copolymer phase diagram.

A change in morphology with weight fraction was also observed for PMMA-*b*-PDMA block copolymers, specifically a change from spherical domains of PDMA in a PMMA matrix to a mixed morphology, with layers at the surface, but spherical structures in the center of the particles (see SI Figure 1). Such mixed morphologies have been previously observed, and are only possible in large block copolymer particles where there is lower spherical confinement.[11,49]

Finally, PMMA-*b*-PBzMA displayed a lamellar-like morphology for the symmetrical copolymer (Figure 6a), but even under heavy staining, no structures were visible for the asymmetric copolymer at PMMA mass fraction 0.78 (see SI Figure 1) which can be explained by the miscibility of the blocks. Such
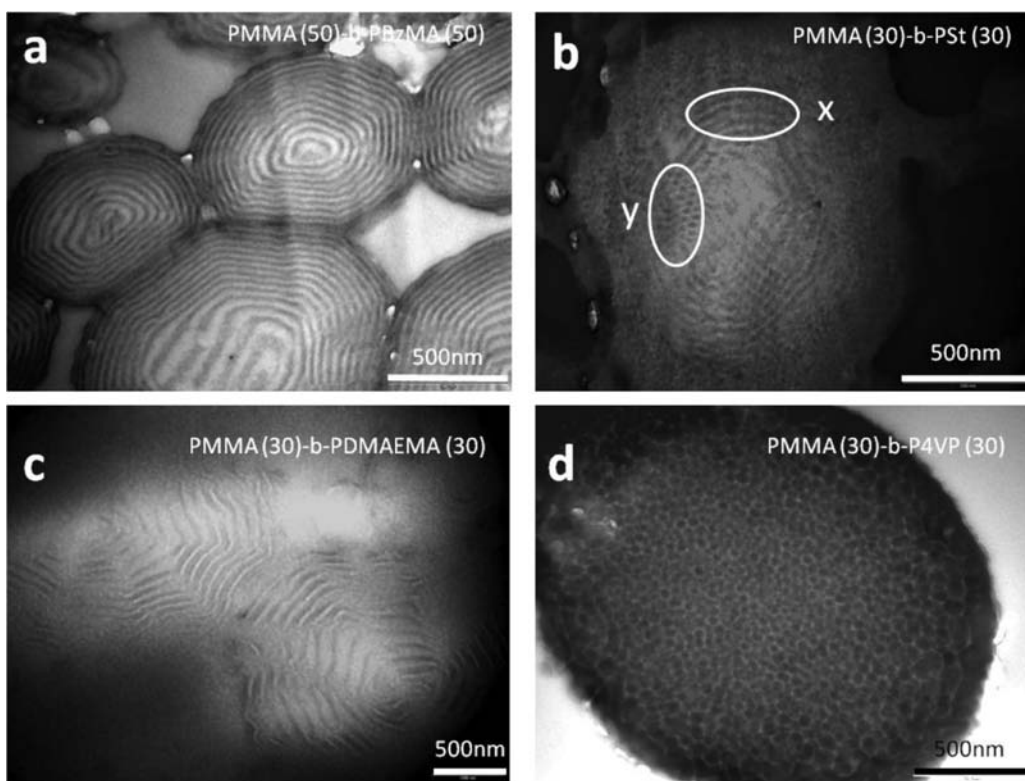
4777

dx.doi.org/10.1021/ja210577h | *J. Am. Chem. Soc.* 2012, 134, 4772−4781

Figure 6. TEM images to show contrast in phase behavior of methacrylate-methacrylate and methacrylate-styrenic block copolymer microparticles: (a) PMMA (50)-*b*-PBzMA (50); (b) PMMA (30)-*b*-PSt (30), note that regions x and y clearly demonstrate the hexagonally packed cylindrical nature of the nanostructured domains; (c) PMMA (30)-*b*-PDMAEMA (30); and (d) PMMA (30)-*b*-P4VP (30). The dark domains are due to RuO_4-stained PBzMA and PSt and I_2-stained PDMAEMA and P4VP.

miscibility is evidenced by DSC data, where only a single T_g is observed, and suggests that in this case the block copolymer system may be close to the weak segregation limit.

Comparison of structurally different block copolymers of the same PMMA mass fractions yielded unexpected results. Symmetrical block copolymers of PMMA-*b*-PBzMA and PMMA-*b*-PDMAEMA show multilayered lamellar morphology, while PMMA-*b*-P4VP and PMMA-*b*-PSt displayed spherical and curved cylindrical domains, respectively (Figure 6). This is surprising, since previous reports show that symmetrical block copolymers should always favor the multilayered lamellar morphology under spherical confinement.[20,50] Additionally, it is well-known that the phase diagram for a block copolymer in the bulk usually shows lamellar domains when the constituent block copolymers are of equal mass fraction.[6]

There has been extensive work on symmetrical PMMA-*b*-PSt copolymers, which are known to form a multilayered structure when confined to a spherical particle of a similar size (1.4 μm)[50] and a lamellar morphology in a thin film.[51] By contrast, the morphology observed from the symmetrical block copolymer PMMA (30)-*b*-PSt (30) synthesized in scCO$_2$ clearly showed curved cylindrical domains of PSt in a PMMA matrix (Figure 6b). It is well-known that addition of homopolymer to a block copolymer system can affect the observed morphology, by preferentially increasing the volume of one phase relative to the other.[52] This effect has also been observed in block copolymer systems confined to a sphere, but only at very high loading (ca. 50 wt %) of homopolymer PMMA.[49] Additionally, formation of structured particles has also been demonstrated by blending of homopolymers using scCO$_2$.[34] Using deconvolution of GPC traces,[53] we have

calculated that the level of "dead" PMMA from the first step in our synthesis is in the range of 5−25 wt % across all samples. This is well below the ~50 wt % of homopolymer which for very similar systems has previously been found to cause a shift from lamellar to cylindrical morphology in symmetrical block copolymers in microparticles. Hence, for these systems, the unexpected morphology we see is unlikely to be caused by contamination with homopolymer.[11,12,49] Recent work investigating block copolymers confined to spherical objects concludes that the degree of spherical confinement, defined by D/L_0 (where D is particle diameter and L is the domain spacing), can have an effect on the phase behavior. However, the particle sizes synthesized by dispersion polymerization in scCO$_2$ are at least an order of magnitude larger than the size required to influence the morphology, which was found when $D/L_0 < 5$.[54]

We hypothesize that in our experiments these unusual morphologies appear because of different sorption of CO$_2$ into the structurally different domains. It is well established that a selective solvent can significantly alter the phase diagram of a given block copolymer system.[55] In this case, CO$_2$ is the continuous phase for the dispersion polymerization, but it also has high solubility in many polymers.[56] For example, P4VP and PSt absorb considerably less CO$_2$ than methacrylates (PMMA, PBzMA and PDMAEMA) over a range of temperatures and pressures.[56] Thus, in a PMMA-*b*-PSt or PMMA-*b*-P4VP block copolymer, CO$_2$ sorption into PMMA will cause an increase in the mass and volume of the PMMA segment relative to the styrenic polymer. In the case of symmetrical PMMA-*b*-P4VP, the PMMA segment will swell more than P4VP, driving the phase diagram to adopt the morphology of spherical P4VP
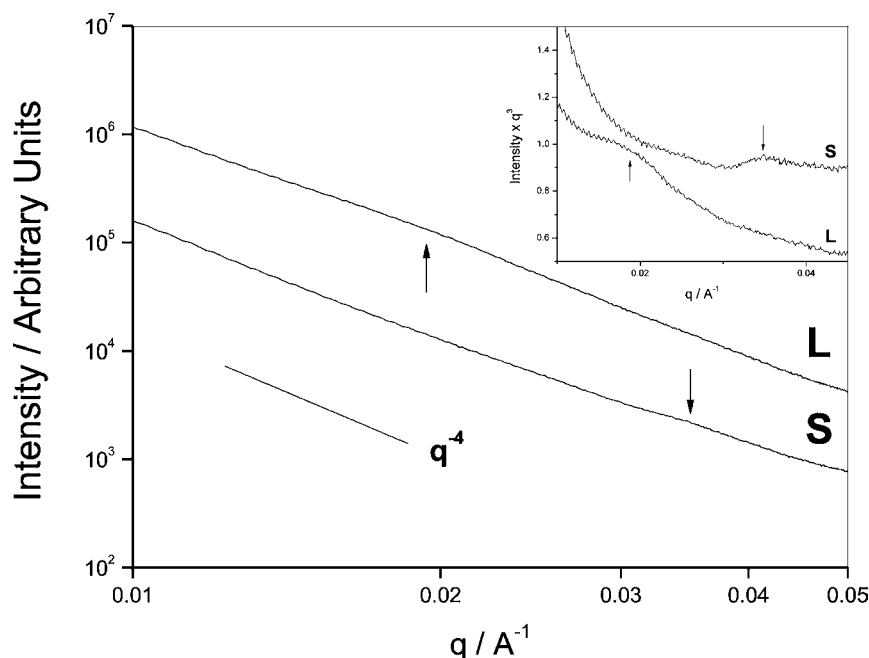
Figure 7. SAXS profiles of PMMA-*b*-P4VP microparticles, (L) PMMA (15)-*b*-P4VP (45) (Lamellar), (S) PMMA (45)-*b*-P4VP (15) (Spherical). The intensities in the main graph have been scaled by increasing orders of magnitude for clarity. The inset shows the SAXS curves plotted as $I \cdot q^3$ as a function of q to enhance the visibility of the peaks in the data. The arrows highlight the position of the peaks in both traces.
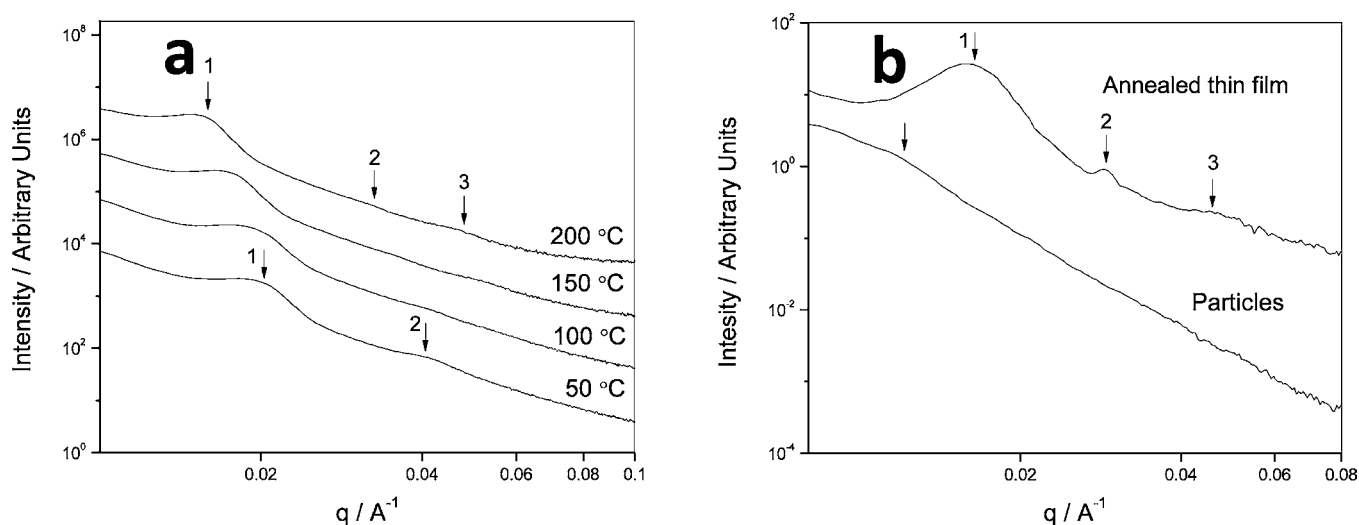

Figure 8. SAXS traces showing the effect of annealing. (a) PMMA (30)-*b*-PDMAEMA (30) microparticles annealed at various temperatures to investigate behavior in the bulk; lamellar morphology is clearly present and at higher temperatures, a third-order peak shows increased order. (b) PMMA (30)-*b*-PSt (30) in particle form and after being solution cast and annealed. In both cases, the intensities of successive traces have been multiplied by increasing orders of magnitude for clarity. The arrows highlight the position of peaks at q = 1,2, and 3, which clearly indicate lamellar morphology in the solvent cast thin film, whereas cylindrical morphology is clearly indicated for the particles obtained directly from scCO$_2$.

domains in a PMMA matrix. In the case of the PMMA (15)-*b*-P4VP (45), the PMMA swells so that its mass fraction becomes closer to 0.5, and hence a multilayered morphology is obtained (Figure 4b). These morphologies are then kinetically trapped when the reaction is quenched. This occurs as temperature is reduced first, preventing the polymers from reordering as the CO$_2$ is removed from the vessel. For symmetrical PMMA-*b*-PBzMA and PMMA-*b*-PDMAEMA copolymer systems, we observe an onion-like structure as expected, since CO$_2$ is absorbed to approximately the same extent into both blocks (Figure 6a,c). In this way, the CO$_2$ drives the morphology toward kinetically trapped structures that depend on a given copolymer composition and the relative affinity for the constituent blocks toward it. This is not surprising, as CO$_2$ has previously been found to have a profound effect on the phase behavior of block copolymer systems.[57]

2.3. SAXS Analysis of Microparticles and Thin Films. To show that the morphologies of the microparticles are consistent throughout the samples and to study the morphology of the block copolymers in the absence of CO$_2$, we carried out small-angle X-ray scattering (SAXS) for a selection of block copolymers. All microparticle samples showed a strongly decaying function, and this is highlighted for two key samples PMMA (15)-*b*-P4VP (45) and PMMA (45)-*b*-P4VP (15)

(Figure 7). The q^{-4} decay (*Porod* scattering) data (Figure 7) clearly show that there are large structures (>ca. 100−200 nm) with sharp interfaces within them and that these are consistent with the overall size of the polymer particles. Superimposed upon this decay are weak, broad inflections (or peaks) from which the mean correlation lengths from SAXS are 18 nm (spherical) and 33 nm (lamellar) which agree well with domain sizes measured from the TEM images (Figure 4, panels a and b, respectively). Moreover, the weak and broad nature of these SAXS maxima suggests that the correlation lengths are highly distributed and/or persist over only a relatively short-range. This again reinforces the particulate nature of the samples and also hints at a variation in domain sizes from edge to center within each individual particle.

Using SAXS, we also observe how the block copolymer samples behave upon thermal annealing. This was not possible with the PMMA-*b*-P4VP copolymers, as degradation was observed under heating. For PMMA (30)-*b*-PDMAEMA (30), the microparticulate samples (TEM Figure 6c) were thermally annealed above the T_g of the component blocks and this caused the peak(s) in the SAXS trace to increase in intensity and sharpen, demonstrating a move to a greater degree of order between the domains in the microparticle (Figure 8a). The SAXS data from these particles correlate well with the lamellar morphology seen in the TEM images (Figure 6c) as evidenced by the relative positions of the first- and second-order peaks present in the scattering profiles (Figure 8a). With increasing annealing temperature, the second-order peak becomes less intense and a third-order peak (at $q \sim 3$ times q of the first-order peak) can be observed, indicative of more symmetrical lamellar structures forming as the block copolymers adopt the morphology over a longer range. In addition, the peaks shift to lower q at higher temperature (note first-, second-, and third-order peaks all shift) which implies that the domain sizes are becoming slightly larger, consistent with a coarsening or ripening of the lamellae as they adopt a more symmetrical morphology as the particles flow or sinter. From these data, it is clear that the observed lamellar morphology in the block copolymer microparticles of PMMA (30)-*b*-PDMAEMA (30) is maintained in the annealed film. Thus, we can again deduce that CO_2 has no direct effect on the phase behavior of the PMMA-methacrylate copolymer, in which we would expect the $scCO_2$ to equally interact with both blocks.

SAXS analysis of microparticles of the symmetrical sample (PMMA (30)-*b*-PSt (30)) (Figure 8b) shows features that match the size order observed by TEM ($d \sim 40$ nm) and are consistent with the size of the cylindrical domains of PS in PMMA (Figure 6b). However, thermal annealing did not reveal any change in peaks under SAXS analysis, probably because of a lack of flow/sintering and, hence, no long-range structure. Instead, the same microparticulate sample was cast as a thin film from a THF solution and annealed at 110 °C. SAXS analysis of this cast film (Figure 8b) shows a very clear lamellar ordering which is exactly what we would expect at this symmetrical block copolymer composition. These data, combined with the TEM image (Figure 6b), demonstrate that for PMMA (30)-*b*-PSt (30) there are different structures present in thin films compared to the microparticles, thus, providing further evidence that $scCO_2$ does indeed modify the block copolymer phase behavior resulting in nanostructures that are different to those formed under thermodynamic control.

■ CONCLUSIONS

We present a reliable and controllable route for the preparation of novel block copolymer microparticles with controlled molecular architecture and nanostructure using a simple one-pot $scCO_2$ approach. Moreover, the whole process is green and environmentally friendly, and yields product with minimal monomer residues.

The method is highly versatile, applicable to both hydrophilic and hydrophobic polymers which are hard and soft in nature (high and low T_g), from monomers with a range of reaction kinetics and solubility characteristics. The RAFT dispersion approach in $scCO_2$ shows excellent control over a range of different monomer types, leading to block copolymers that might be difficult or impossible to achieve in a microparticulate form through more conventional routes. A wide range of nanostructured block copolymer morphologies are accessible, and can be manipulated by control of the mass fractions of the blocks, as well as by changing the constituent blocks, suggesting an effect of CO_2 sorption on the block copolymer phase behavior. This simple one-pot process leads to hierarchical materials that have controlled structure on two length scales, which will be valuable for future application.

■ ASSOCIATED CONTENT

ⓢ Supporting Information

TEM images of other copolymers and unstained particles, SEM and GPC data for PMMA samples and ^{1}H NMR spectra of block copolymers. This material is available free of charge via the Internet at http://pubs.acs.org.

■ AUTHOR INFORMATION

Corresponding Author
steve.howdle@nottingham.ac.uk

Notes
The authors declare no competing financial interest.

■ ACKNOWLEDGMENTS

■ REFERENCES

(1) Sundberg, D. C.; Durant, Y. G. *Polym. React. Eng.* **2003**, *11*, 379.
(2) Lu, Z.; Liu, G.; Phillips, H.; Hill, J. M.; Chang, J.; Kydd, R. A. *Nano Lett.* **2001**, *1*, 683.
(3) Hamley, I. W. *Nanotechnology* **2003**, *14*, R39.
(4) Bockstaller, M.; Kolb, R.; Thomas, E. L. *Adv. Mater.* **2001**, *13*, 1783.
(5) Gourevich, I.; Field, L. M.; Wei, Z.; Paquet, C.; Petukhova, A.; Alteheld, A.; Kumacheva, E.; Saarinen, J. J.; Sipe, J. E. *Macromolecules* **2006**, *39*, 1449.
(6) Bates, F. S. *Science* **1991**, *251*, 898.
(7) Bates, F. S.; Fredrickson, G. H. *Phys. Today* **1999**, *52*, 32.
(8) Castelletto, V.; Hamley, I. W. *Curr. Opin. Solid State Mater. Sci.* **2004**, *8*, 426.
(9) Thurn-Albrecht, T.; Steiner, R.; DeRouchey, J.; Stafford, C. M.; Huang, E.; Bal, M.; Tuominen, M.; Hawker, C. J.; Russell, T. *Adv. Mater.* **2000**, *12*, 787.

(10) Arsenault, A. C.; Rider, D. A.; Tétreault, N.; Chen, J. I. L.; Coombs, N.; Ozin, G. A.; Manners, I. *J. Am. Chem. Soc.* **2005**, *127*, 9954.

(11) Jeon, S.-J.; Yi, G.-R.; Koo, C. M.; Yang, S.-M. *Macromolecules* **2007**, *40*, 8430.

(12) Jeon, S.-J.; Yi, G.-R.; Yang, S.-M. *Adv. Mater.* **2008**, *20*, 4103.

(13) Higuchi, T.; Tajima, A.; Motoyoshi, K.; Yabu, H.; Shimomura, M. *Angew. Chem., Int. Ed.* **2008**, *47*, 8044.

(14) Okubo, M.; Takekoh, R.; Izumi, J. *Colloid Polym. Sci.* **2001**, *279*, 513.

(15) Okubo, M.; Takekoh, R.; Saito, N. *Colloid Polym. Sci.* **2003**, *281*, 945.

(16) Okubo, M.; Takekoh, R.; Saito, N. *Colloid Polym. Sci.* **2004**, *282*, 1192.

(17) Yabu, H.; Higuchi, T.; Ijiro, K.; Shimomura, M. *Chaos* **2005**, *15*, 047505.

(18) Zhang, K.; Yu, X.; Gao, L.; Chen, Y.; Yang, Z. *Langmuir* **2008**, *24*, 6542.

(19) Nicolas, J.; Ruzette, A.-V.; Farcet, C.; Gérard, P.; Magnet, S.; Charleux, B. *Polymer* **2007**, *48*, 7029.

(20) Kagawa, Y.; Minami, H.; Okubo, M.; Zhou, J. *Polymer* **2005**, *46*, 1045.

(21) Kitayama, Y.; Kagawa, Y.; Minami, H.; Okubo, M. *Langmuir* **2010**, *26*, 7029.

(22) Higuchi, T.; Tajima, A.; Yabu, H.; Shimomura, M. *Soft Matter* **2008**, *4*, 1302.

(23) Higuchi, T.; Tajima, A.; Motoyoshi, K.; Yabu, H.; Shimomura, M. *Angew. Chem., Int. Ed.* **2009**, *48*, 5125.

(24) Higuchi, T.; Motoyoshi, K.; Sugimori, H.; Jinnai, H.; Yabu, H.; Shimomura, M. *Macromol. Rapid Commun.* **2010**, *31*, 1773.

(25) Li, L.; Matsunaga, K.; Zhu, J.; Higuchi, T.; Yabu, H.; Shimomura, M.; Jinnai, H.; Hayward, R. C.; Russell, T. P. *Macromolecules* **2010**, *43*, 7807.

(26) Wei, R.; Luo, Y.; Li, Z. *Polymer* **2010**, *51*, 3879.

(27) Herrera, V.; Pirri, R.; Asua, J. M.; Leiza, J. R. *J. Polym. Sci., Part A: Polym. Chem.* **2007**, *45*, 2484.

(28) Li, Y. T.; Armes, S. P. *Angew. Chem.-Int. Edit.* **2010**, *49*, 4042.

(29) Erdmenger, T.; Guerrero-Sanchez, C.; Vitz, J.; Hoogenboom, R.; Schubert, U. S. *Chem. Soc. Rev.* **2010**, *39*, 3317.

(30) Davies, O. R.; Lewis, A. L.; Whitaker, M. J.; Tai, H. Y.; Shakesheff, K. M.; Howdle, S. M. *Adv. Drug Delivery Rev.* **2008**, *60*, 373.

(31) Zetterlund, P. B.; Kagawa, Y.; Okubo, M. *Chem. Rev.* **2008**, *108*, 3747.

(32) Kendall, J. L.; Canelas, D. A.; Young, J. L.; DeSimone, J. M. *Chem. Rev.* **1999**, *99*, 543.

(33) Woods, H. M.; Silva, M.; Nouvel, C.; Shakesheff, K. M.; Howdle, S. M. *J. Mater. Chem.* **2004**, *14*, 1663.

(34) Young, J. L.; DeSimone, J. M. *Macromolecules* **2005**, *38*, 4542.

(35) Zetterlund, P. B.; Aldabbagh, F.; Okubo, M. *J. Polym. Sci., Part A: Polym. Chem.* **2009**, *47*, 3711.

(36) Thurecht, K. J.; Howdle, S. M. *Aust. J. Chem.* **2009**, *62*, 786.

(37) Thurecht, K. J.; Gregory, A. M.; Wang, W. X.; Howdle, S. M. *Macromolecules* **2007**, *40*, 2965.

(38) Thurecht, K. J.; Gregory, A. M.; Villarroya, S.; Zhou, J. X.; Heise, A.; Howdle, S. M. *Chem. Commun.* **2006**, 4383.

(39) Lai, J. T.; Filla, D.; Shea, R. *Macromolecules* **2002**, *35*, 6754.

(40) Wang, W. X.; Giles, M. R.; Bratton, D.; Irvine, D. J.; Armes, S. P.; Weaver, J. V. W.; Howdle, S. M. *Polymer* **2003**, *44*, 3803.

(41) Thurecht, K. J.; Heise, A.; deGeus, M.; Villarroya, S.; Zhou, J. X.; Wyatt, M. F.; Howdle, S. M. *Macromolecules* **2006**, *39*, 7967.

(42) Zhong, M. J.; Matyjaszewski, K. *Macromolecules* **2011**, *44*, 2668.

(43) Gregory, A. M.; Thurecht, K. J.; Howdle, S. M. *Macromolecules* **2008**, *41*, 1215.

(44) Guan, Z. B.; Combes, J. R.; Menceloglu, Y. Z.; Desimone, J. M. *Macromolecules* **1993**, *26*, 2663.

(45) Shoji, M.; Eguchi, M.; Layman, J. M.; Cashion, M. P.; Long, T. E.; Nishide, H. *Macromol. Chem. Phys.* **2009**, *210*, 579.

(46) Luo, Y. W.; Wang, X. G.; Zhu, Y.; Li, B. G.; Zhu, S. P. *Macromolecules* **2010**, *43*, 7472.

(47) Perrier, S.; Takolpuckdee, P. *J. Polym. Sci., Part A: Polym. Chem.* **2005**, *43*, 5347.

(48) Grignard, B.; Jerome, C.; Calberg, C.; Jerome, R.; Wang, W. X.; Howdle, S. M.; Detrembleur, C. *Macromolecules* **2008**, *41*, 8575.

(49) Okubo, M.; Saito, N.; Takekoh, R.; Kobayashi, H. *Polymer* **2005**, *46*, 1151.

(50) Tanaka, T.; Saito, N.; Okubo, M. *Macromolecules* **2009**, *42*, 7423.

(51) Yang, X. M.; Peters, R. D.; Nealey, P. F.; Solak, H. H.; Cerrina, F. *Macromolecules* **2000**, *33*, 9575.

(52) Tanaka, H.; Hasegawa, H.; Hashimoto, T. *Macromolecules* **1991**, *24*, 240.

(53) Gao, H. F.; Tsarevsky, N. V.; Matyjaszewski, K. *Macromolecules* **2005**, *38*, 5995.

(54) Li, S. B.; Chen, P.; Zhang, L. X.; Liang, H. J. *Langmuir* **2011**, *27*, 5081.

(55) Lodge, T. P.; Pudil, B.; Hanley, K. J. *Macromolecules* **2002**, *35*, 4707.

(56) Zhang, Y.; Gangwani, K. K.; Lemert, R. M. *J. Supercrit. Fluids* **1997**, *11*, 115.

(57) RamachandraRao, V. S.; Gupta, R. R.; Russell, T. P.; Watkins, J. J. *Macromolecules* **2001**, *34*, 7923.